Simulation of Plastic Deformation in Glassy Polymers: Atomistic and Mesoscale Approaches

SERGEI SHENOGIN,[1,2] RAHMI OZISIK[1,2]

[1]Rensselaer Nanotechnology Center, Rensselaer Polytechnic Institute, Troy, New York 12180

[2]Department of Materials Science and Engineering, Rensselaer Polytechnic Institute, Troy, New York 12180

Received 11 August 2004; revised 16 November 2004; accepted 8 December 2004
DOI: 10.1002/polb.20389
Published online in Wiley InterScience (www.interscience.wiley.com).

ABSTRACT: The mechanism of deformation in glasses is very different from that of crystals, even though their general behavior is very similar. In this study, we investigated the deformation of polycarbonate on the atomistic scale with molecular dynamics and on the continuum scale with a new simulation approach. The results indicated that high atomic/segmental mobility and low local density enabled the formation (nucleation) of highly deformed regions that grew to form plastic defects called *plastic shear transformations*. A continuum-scale simulation was performed with the concept of plastic shear transformations as the basic region of deformation. The continuum simulations were able to predict the primary and secondary creep behavior. The slope of the secondary creep depended on the interactions between the plastic shear transformations. © 2005 Wiley Periodicals, Inc. J Polym Sci Part B: Polym Phys 43: 994–1004, 2005

Keywords: glassy polymers; molecular dynamics; multiscale; plastic deformation; polycarbonates; Monte Carlo

INTRODUCTION

The physics of disordered materials is an extremely important problem that still needs further study. The issues involve theoretical, experimental, and computational studies of structural, thermodynamic, mechanical, and other properties of glasses. The main difficulty of the disordered state arises from the fact that powerful methods of solid-state physics, such as dislocation theory and dynamic analysis,[1] developed for the crystalline state are not applicable to glasses. For systems without long-range order, a different approach must be used in which the localization of the macroscopic properties should be considered.[2–4]

The deformation of ordered systems, such as crystals, has been studied extensively, and established theories of crystalline plasticity have been well known since the 1930s.[5,6] The dislocation theories of plasticity give reliable explanations for the macroscopic deformation behavior of crystals (yielding, strain softening, and hardening) and for structural changes caused by deformation (development of shear bands, etc.).[1] The macroscopic plastic behavior of polymer glasses, at first glance, is very similar to that of crystals. Deformed polymer glasses exhibit yielding, strain softening, and hardening processes; however, recent experimental results obtained from deformation calorimetric studies, residual strain recovery rate measurements, thermally stimulated creep, differential scanning calorimetry, and so forth suggest that the internal mechanisms of plastic flow in glasses and crystalline materials are drastically different. In contrast to crystals, the nucleation and initial development of plastic deformation in

Correspondence to: R. Ozisik (E-mail: ozisik@rpi.edu)

Journal of Polymer Science: Part B: Polymer Physics, Vol. 43, 994–1004 (2005)

glasses are not accompanied by heat release.[7] It has been suggested that all the external work performed on a deformed sample is stored as internal energy in localized plastic structural defects, which we call *plastic shear transformations* (PSTs).[8–15] The difference between the dislocations in crystals and PSTs in glasses is in the high localization of the latter: once initiated, a PST cannot grow or propagate through the disordered structure. Therefore, the local PST is similar to the nucleus of the regular dislocation loop in crystals, and the distribution of line plastic defects in a crystal is replaced with the distribution of point plastic defects in the glass. Naturally, the formation of a single PST requires much more energy (per unit of stored inelastic strain) than the formation of a regular dislocation line in the crystal. Along with this approach, a number of theories (the latest one is called the shear transformation zone theory)[16] have been suggested with different assumptions about the geometry of local plastic defects in glasses, their internal energy, and their interaction energy. With the use of fitting parameters, most of these theories can satisfactorily describe the experimental macroscopic deformation of polymer glasses. However, modern experimental techniques cannot provide information about the possible structures of plastic defects in glasses. Standard structural methods such as electron microscopy, atomic force microscopy, and X-ray analysis cannot detect the existence of a PST or measure its dimension and shape. At low global strains, PSTs are structurally indistinguishable from the surrounding glass, and only internal strain distribution on the scale of approximately 10 nm could reveal them. More indirect methods have been used to measure the changes in the free volume distribution (i.e., positron annihilation),[17–20] vibrational spectrum (i.e., Raman spectroscopy), and molecular segment orientation (solid-state NMR)[21–23] due to plastic deformation of polymer glasses. These valuable results, however, cannot tell much about the micromechanism of plasticity in glasses, that is, what kind of plastic defects are produced by deformation.

Because of these difficulties, atomic-level computer simulations are very promising. When the deformation of a glassy polymer exceeds a strain of a few percent, irreversible changes take place (plastic events). It is possible to obtain information on dynamic processes with static energy minimization of a series of perturbed structures, and these techniques are termed *quasi-static*. Such a simulation was performed by Mott et al.[24] on atactic polypropylene. A small extensional strain step was applied to a minimized starting structure with three-dimensional periodicity. Subsequent minimization caused the system to search for a new minimum energy conformation. The results of this simulation revealed jumps in the stress–strain curve that corresponded to an excessive rearrangement of the entire structure. The stress–strain behavior was reversible (elastic) before the jumps but was irreversible (plastic) after the jumps took place. Moreover, the plastic events corresponded to a global rearrangement of the chains and were not restricted to a local region or a single chain. Argon et al.[25] calculated the region going through plastic deformation to be approximately 10 nm. Simulations performed with Monte Carlo (MC)[26,27] or molecular dynamics (MD)[28,29] techniques often give reasonable qualitative results for the plastic deformation behavior of model glasses. If the correct force field is selected, the yielding at the correct level of stress and strain hardening at higher deformation can be simulated, and experimental stress–strain diagrams can be reproduced.[28,30] However, direct atomic-level simulations of plastic deformation in polymer glasses cannot reproduce the correct energy storage for the deformed structure and thermally stimulated recovery of deformation. A probable reason is that even with up-to-date computers, the size of the amorphous structure that may be simulated is limited to nanometers. As a result, a long-range interaction between plastic defects is excluded from consideration, and so the typical deformational behavior of a simulated structure is very different from the reality.

Instead of performing atomistic simulations, we have used a multiscale approach to simulate plastic deformation in polycarbonate (PC). Multiscale modeling has already received attention,[31] particularly for the study of plastic deformation, brittle fracture,[32] crack-tip propagation,[33] and other problems in solids.[34,35] Ortiz[35] reviewed selected issues of micromechanical models, with a particular emphasis on multiple-scale problems. Tadmor et al.[36,37] used multiscale modeling to study the nanoindentation of an oriented aluminum substrate, among other things. Shenoy et al.[38] recently presented an extension to the method defined by Tadmor et al.[36,37] to study the interaction between grain boundaries and dislocations.

Miller and Phillips[39] used atomistic and continuum levels to compare the Pierels dislocation model with atomistic results. Rafii-Tabar et al.[40] studied crack propagation by combining MD and the finite-element method. In this approach, MD was used to drive the crack tip forward, and the finite-element method was used to calculate the displacements of the atoms at the boundary of an atomistic lattice. Gao and Klein[41] recently proposed a different approach in which interacting material particles are used to define the cohesive behavior of the system, which ranges from interatomic bonding to macroscopic ductile failure. Other attempts at combining different levels of description can be found in several areas, such as calculations of flow in dense fluids[42] and protein simulations.[43,44]

SIMULATION SETUP

In this work, we performed two simulations at two distinct length scales: atomistic and continuum levels. The two simulations were connected through PSTs: the geometric characteristics of the PSTs were defined at the end of the atomistic-level simulations, and then a coarse-grained PST description was used in the continuum-level simulation. In this section, we describe the details of our simulation approach on both length scales.

Atomistic-level simulations of glassy polymer structures were performed with a recently developed in-house code called Macromolecular Reality.[45,46] Macromolecular Reality mimics the Discover module in Insight II, Cerius2, and Materials Studio programs (Accelrys, Inc.). In Macromolecular Reality, we have access to CFF91,[47] PCFF,[48] PCFF with second-order cross terms, and our own specialized force fields. CFF91 and PCFF are second-generation force fields derived from *ab initio* models. CFF91 has been parameterized against a wide range of experimental observables for organic compounds containing H, C, N, O, S, P, halogen atoms and ions, alkali metal cations, and several biochemically important divalent metal cations. PCFF is based on CFF91 and is extended to have a broad coverage of organic polymers, metals, and zeolites. We use the PCFF force field developed by Suter et al.[49] Macromolecular Reality also includes a graphical user interface created in our laboratory (called XenoView)[45] and uses common file formats.

Several PC structures were created with a method first proposed by Muller et al.[49] This method (the software code is named PolyPack) consists of a heuristic search algorithm in the space of torsion angles, which automatically delivers the correct conformational statistics of the chains. The performance and efficiency of this method have been previously verified for polyethylene and polystyrene.[49] In comparison with similar methods,[50–55] PolyPack gives good initial structures because its search algorithm is based on maintaining rotational-isomeric-state probabilities.

In the MD simulations, all the atoms were explicitly defined. We used a 0.5-fs time step in all simulations. The typical computational cell size was about 3–4 nm, which assumes 3000–5000 explicit C, O, and H atoms. The molecular weight of all the chains was 6352 g/mol (25 repeating units); the number of chains varied. With three-dimensional periodic boundary conditions at the standard temperature and pressure, the density of the models stabilized in the range of 1.142–1.148 g/cm^3 for PC, which is very close to the experimental density. These MD models were used to analyze the spatial distribution of the local strains and stresses that arise in a PC sample when it is stretched, compressed, or deformed by an external shear.

After the creation of the initial structure and equilibration, each system was equilibrated (with no external stress) for at least 30–40 ps for proper averaging and then was tested under various levels of deformation (external stress). After averaging, the nearest neighbors of each atom were defined with Voronoi polyhedral analysis, which essentially described the cage of each atom. Our recent analysis (with PC) showed that each atom typically has 6–10 nearest neighbors. Then, the structure was deformed by a small constant external stress (creep test), the level of the stress being well below the yield stress threshold. Typical global strains of 1–5% were sought to analyze the initial stages of deformation. Also, a small value of deformation ensured that most atoms did not experience a change in their nearest neighbors and that the structure could be stable under stress for 20 ps, which was required for time averaging in the deformed stage. From the displacement of nearest neighbors in the deformed state, local strain tensor, $\|\varepsilon\|$, can be obtained for each "cage" from the minimization of the following equation:

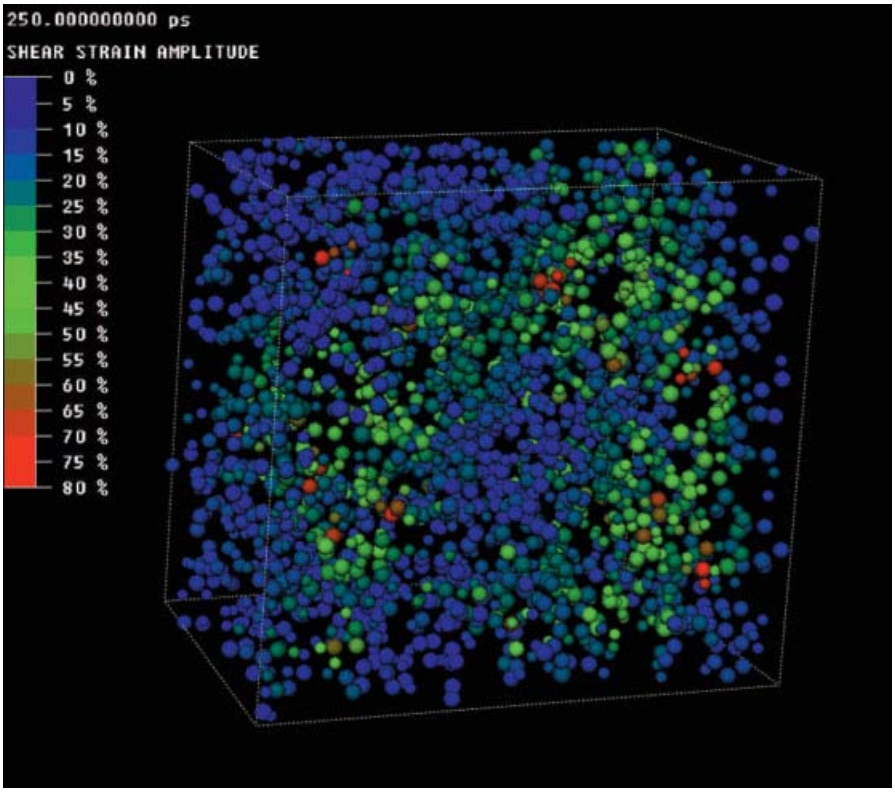

Figure 1. Distribution of the local shear strain in PC at the end of 250 ps under tensile deformation (along the horizontal axis). The global strain is 3.8%. The atoms are colored according to the shear strains that their surroundings (as defined by their Voronoi volume) are experiencing.

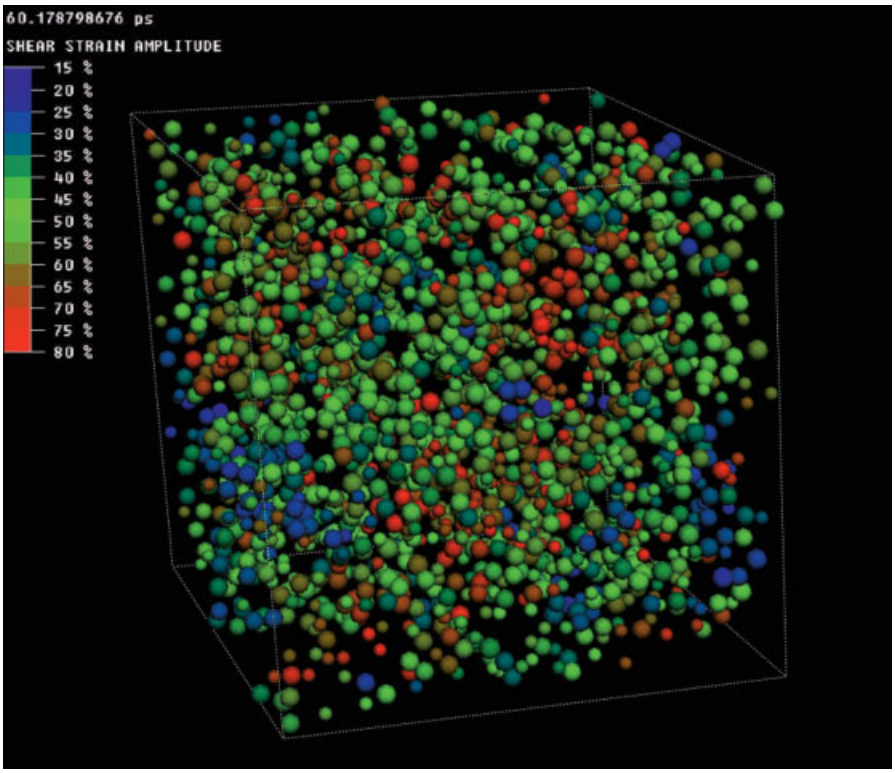

Figure 2. Distribution of the local shear strain in PC as a result of hydrostatic deformation. The global strain is 9.2%. The atoms are colored according to the shear strains that their surroundings (as defined by their Voronoi volume) are experiencing.

$$\Delta R^2 = \frac{1}{N}\sum_{i=1}^{N}(\Delta\vec{r}_{\mathrm{def},i} - \|\varepsilon\| \cdot \vec{r}_{0,i})^2 \qquad (1)$$

where N is the number of nearest neighbors, $r_{\mathrm{def},i}$ is the actual relative displacement of each neighbor after deformation, $r_{0,i}$ is the relative position of each neighbor, and the summation is performed over all the nearest neighbors. Parameter ΔR^2 is the accuracy of local strain field with respect to the constant tensor $\|\varepsilon\|$ with six independent components. The spatial distribution of the (ε) components were analyzed for each deformation mode. The goal was to find correlations between the local packing and local shear strain and to detect the localization of shear strain that could be considered a plastic defect or PST.

To perform the continuum-level simulations, we built a three-dimensional MC model. In this model, the plastic flow in a glassy polymer is treated as a stochastic sequence of local PSTs. The size and geometry of the local PSTs were introduced according to the results of our MD simulations and experimental data.[56] We performed preliminary simulations in which the PSTs were defined as flat ellipsoid regions within an amorphous structure that could undergo pure shear deformation when external stress was applied. The energy required for such transformations was calculated from the continuum mechanics:[57]

$$E_{\mathrm{el}} = \frac{V_0\varepsilon_0^2 E}{2(1+v)}\left[1 + \frac{\pi c_0(2-v)}{4a_0(1-v)}\right] \qquad (2)$$

where E_{el} is the energy; V_0 is the initial volume, c_0 is the thickness, and a_0 is the diameter of the PST; ε_0 is the constant local strain (pure shear); E is Young's modulus; and v is Poisson's ratio. E_{el} is calculated from the elastic strain field at large distances away from the PSTs, and the energy stored in the PST core is neglected. This approximation is valid as long as no large density change is involved in the transformation, and the dimensions of the core are small in comparison with typical distances at which PSTs interact.

The elastic displacement field (u_i) produced by a single PST at point $\boldsymbol{r}$ was also calculated[57] as shown in Eqs 3 and 4:

$$u_i(r) = \frac{V_0}{4\pi(1-v)r^2}(\varepsilon^o_{jk} g_{ijk}) \qquad (3)$$

where

$$g_{ijk} = (1-2v)[\delta_{ij}l_k + \delta_{ik}l_j] + 3l_i l_j l_k \qquad (4)$$

and δ is the Kronecker delta, ε^o is the PST shear strain tensor, and l is the unit vector from PST to the point of observation at $r = (l_i = r_i/r)$. The energy of interaction (E_{int}) between PST and external elastic strain field ($\varepsilon^{\mathrm{ext}}$) was obtained as follows:

$$E_{\mathrm{int}} = -\frac{V_0 E}{1+v}\varepsilon^0_{ij}\varepsilon^{ext}_{ij} \qquad (5)$$

Equations 3–5 provide an expression for the interaction energy between two PST defects, which depends only on their relative position and orientation.

Instead of the explicit-atom model, the elastic continuum model with embedded PSTs representing sites with high local shear strain is more suitable, especially at small deformations. In the continuum model, the internal strain and stress distribution in the sample were analytically calculated. This resulted in an effective computer code, and much larger simulation box sizes (up to 1 μm, holding up to 50,000 PSTs) could be achieved in comparison with the explicit-atom MD simulations. A standard Metropolis MC algorithm was used for the simulation of plastic flow at various temperatures and under constant external stress conditions.

Before the MC simulations were performed, the concentration of PSTs and their size and orientation distributions had to be supplied to the model. These parameters could not be obtained from our MD simulations, so in this study we considered a single size for all PSTs. We should point out that the MC simulations do not refer to a real system but are model simulations that can be applied in general to all glasses. In this study, we attempted to verify the concept of PSTs and that the use of PSTs could result in reasonable deformation behavior.

The typical MC cell size was 100 nm × 100 nm × 100 nm, with 5000 PSTs uniformly distributed and randomly oriented. Each PST was represented as a flat ellipsoid with 4 Å thickness and 4 nm diameter. The size of the PSTs was used only for the calculation of their energy and elastic field with eqs 2–5. Elastic constants of the surrounding medium were chosen to be close enough to typical macroscopic values for glassy polymers (modulus = 1.0 GPa, $v = 0.45$).

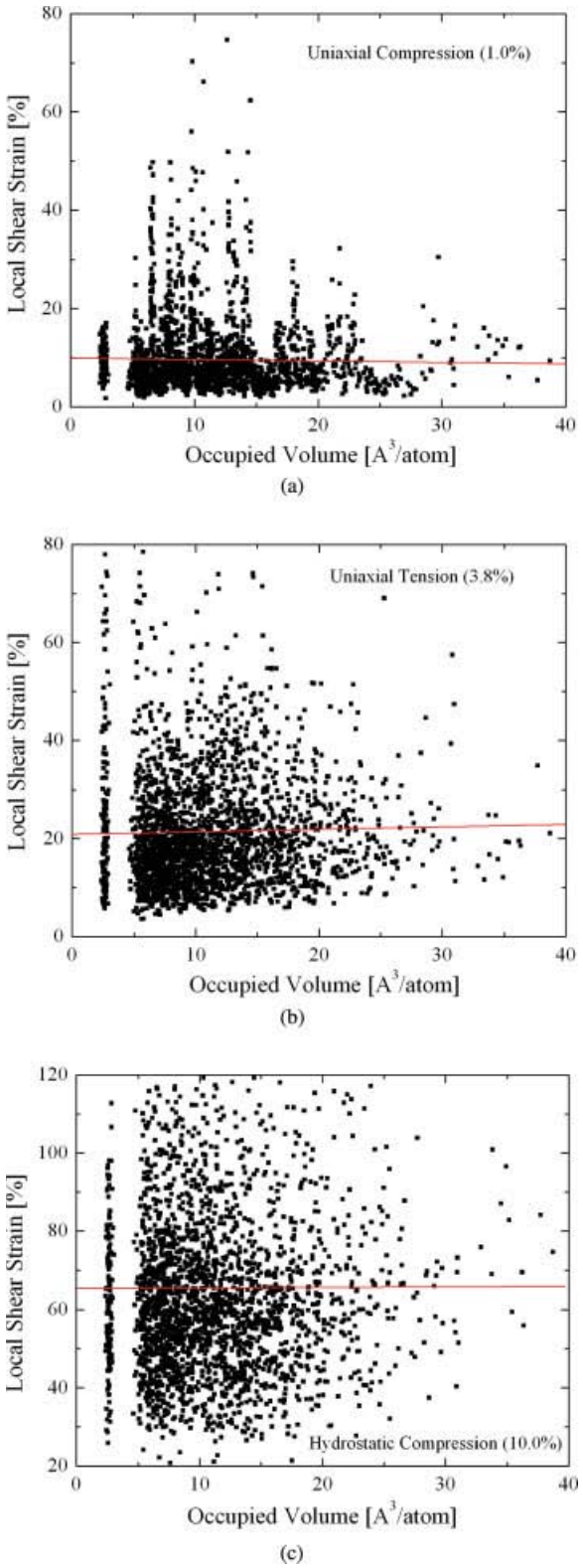

Figure 3. Local shear strain experienced by the Voronoi volume of each atom versus the initial occupied volume (local packing) for (a) 3.8% uniaxial tension, (b) 1.0% uniaxial compression, and (c) 10% hydrostatic compression.

RESULTS AND DISCUSSION

Atomic-Level Simulations

Our atomistic simulations showed a great difference between the global and local strains. This is shown in Figure 1, in which each atom is color-coded according to the local shear strain in its surroundings. In this example, the global strain is 3.8% under uniaxial tension at the end of 250 ps of simulation, whereas the local shear strain (defined by eq 1) reaches as high as 80% for a small number of atoms. Further analysis shows that the atoms that have extremely high local shear strains also have high initial mobility. This suggests that the regions that have atoms (or segments) that have high mobility deform more easily. Figure 1 also shows that there is a localization of shear strain around certain regions, which are explored later in this section. On the other hand, when a hydrostatic stress is applied, no such localization of shear strains can be observed (see Fig. 2), and this indicates that a shear component (of applied stress) is required to create the localized regions of high local shear strains.

Figure 3 shows the correlation between the local shear strain and local packing density for three modes of deformation: uniaxial tension, uniaxial compression, and hydrostatic compression. Each data point represents the Voronoi volume of an atom in the simulation box. In all deformation modes, the atoms experience a wide

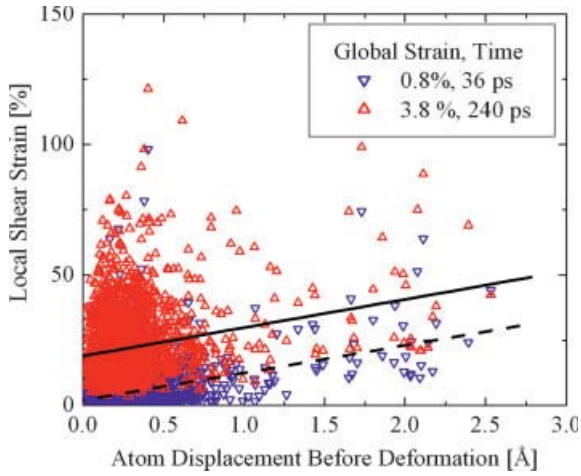

Figure 4. Correlation between the local shear strain and atom mobility. The x axis shows the displacement of the atoms before the external stress is applied. Each point corresponds to an atom in the simulation box.

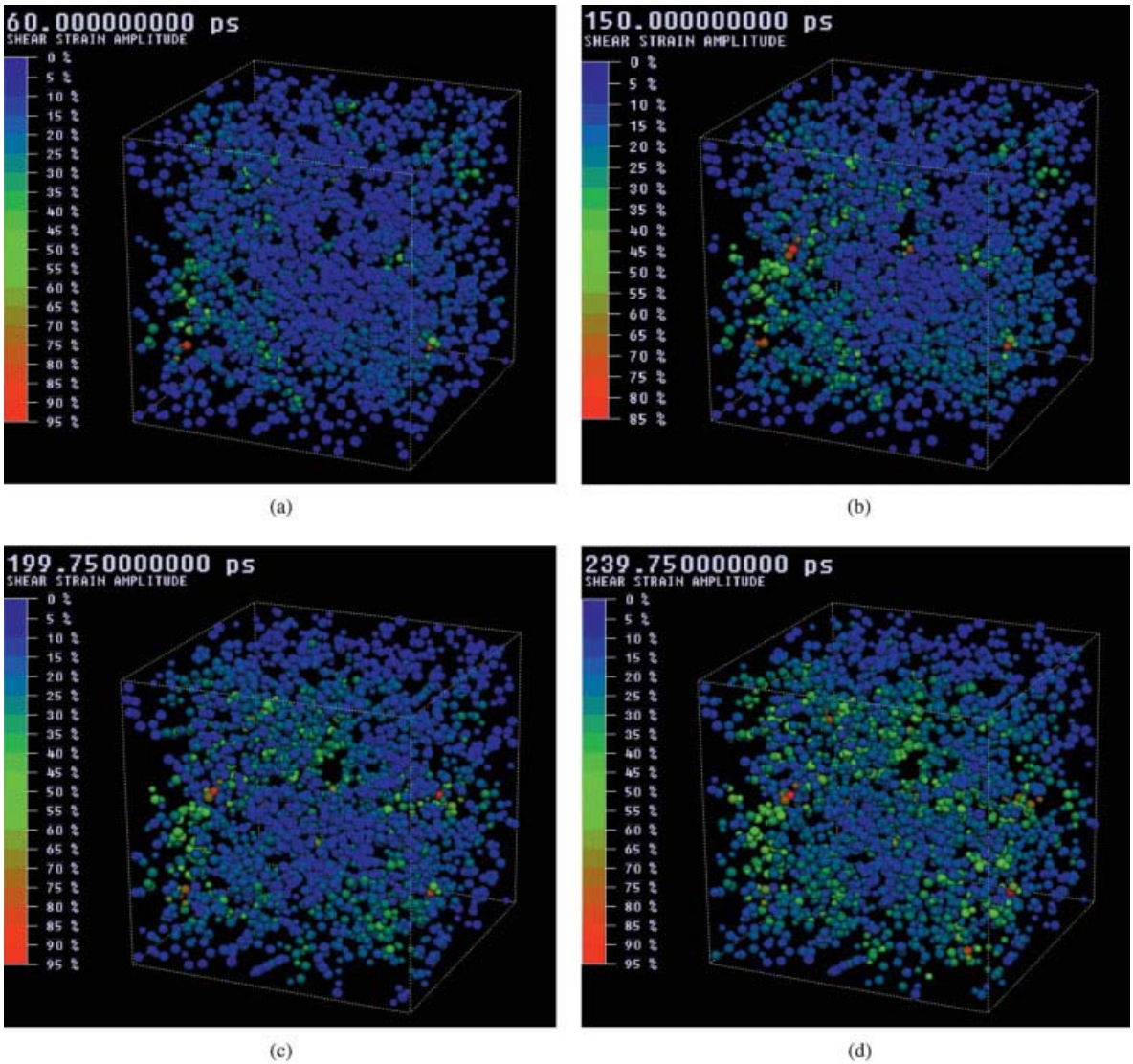

Figure 5. Nucleation and growth of inelastic shear strain in PC at (a) 1.5, (b) 2.5, (c) 3.2, and (d) 4.0% global strain.

range of local shear strains within their Voronoi volume. Even the atoms with the smallest Voronoi volumes experience a wide range of local shear strains. The solid line shown in Figure 3 is a linear least-squares fit to the data and has a small positive slope, which indicates that there is a weak correlation between the packing density and local shear. This result seems unusual because it can be assumed that regions of low density can be deformed more easily than high-density regions because of the higher mobility expected in the low-density regions. A similar result was obtained by Capaldi et al.,[29] who observed no correlation between the local density and deformation-induced mobility. The results obtained by Capaldi et al. were at high global strains (up to 100%), whereas our results were obtained at low global strains. These results indicate that although there is a small correlation between the local density and local shear strains, the local density (local packing) does not affect the deformation mechanism very strongly.

Figure 4 shows the local shear strains experienced by the Voronoi volume of each atom at two levels of global deformation as a function of the atom mobility before the application of external stress. Neighborhoods of atoms with low initial mobility (as expressed by the x axis) experience low shear strains. As shown by the

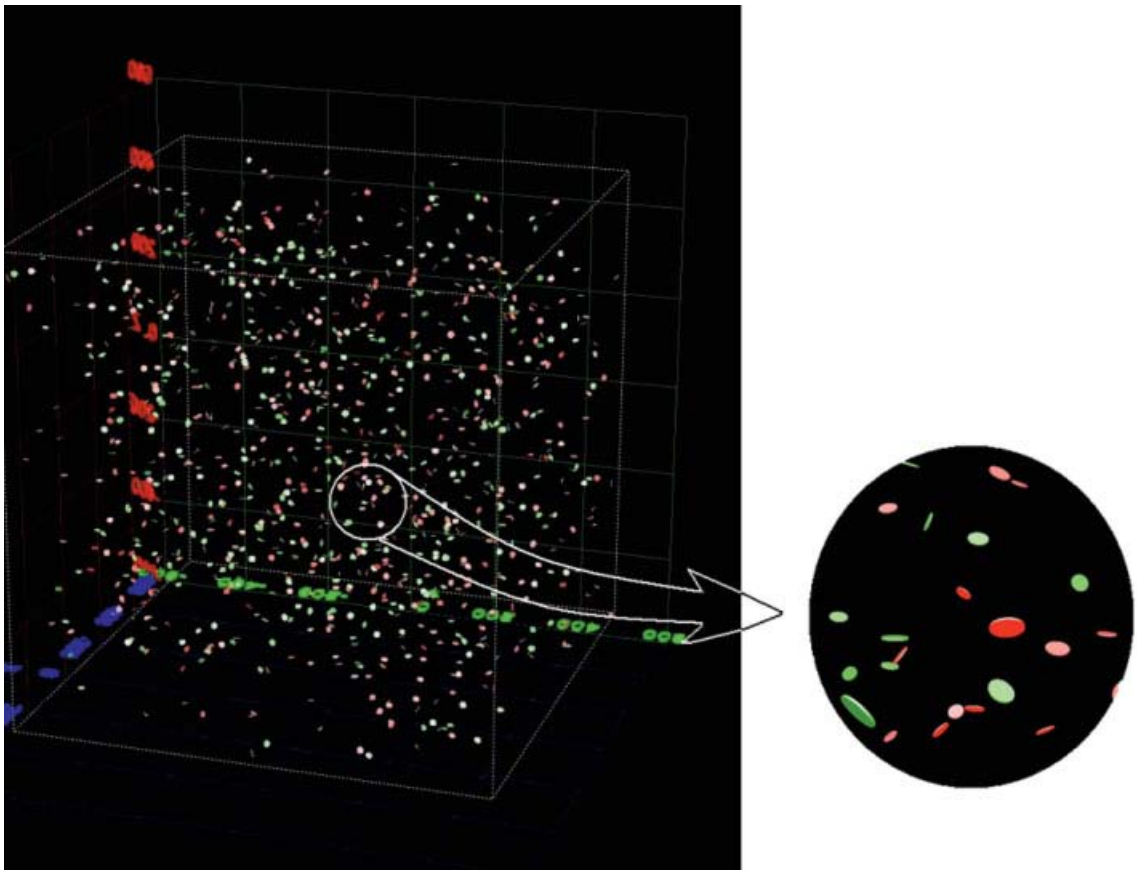

Figure 6. PSTs represented as flat ellipsoids during the continuum simulation. The simulation box shown here is 100 nm × 100 nm × 100 nm and contains a small number of PSTs for easy viewing.

solid lines (linear fits to the data), there is a much stronger correlation between the atom mobility and shear strain localization than between the local density and local shear strain. The findings of Figure 3 and 4 indicate the interplay of the local density, local mobility, and local shear deformation. Although there is a weak correlation between the local density and mobility, this is not the only factor that affects local mobility. The mobility is affected by the local density and chemical structure. Therefore, we believe that it is essential to have a flexible segment to develop an inelastic strain in the structure. Then, these highly mobile regions act as nucleation sites for plastic deformation.

The nucleation sites formed under shear strain grow as the shear strain levels increase (see Fig. 5) and form a region that we call a PST.[11] The shapes of the PSTs are flat and elliptical and are oriented along the direction of the largest shear stress (45° to the direction of the uniaxial stress). Such localization has not been observed under hydrostatic stress (the deformation regions are diffuse). This suggests that external shear stress is required to enable the interaction of the nuclei and the formation of a localized PST.

Continuum-Level Simulations

In our MC simulation, the PSTs are represented as flat ellipsoids approximately 3–5 Å thick and approximately 4 nm in diameter. These ellipsoids can be deformed elastically according to eqs 2–5. A sample box is shown in Figure 6. To compare our MC simulation results, we show experimental results of a creep test for PC in Figure 7. However, our MC simulation results are for a model glassy polymer system rather than a real system. Therefore, only a qualitative comparison can be performed at this point. Typical experimental creep curves for glassy polymers have a primary part with a gradually decreasing deformation rate and a secondary

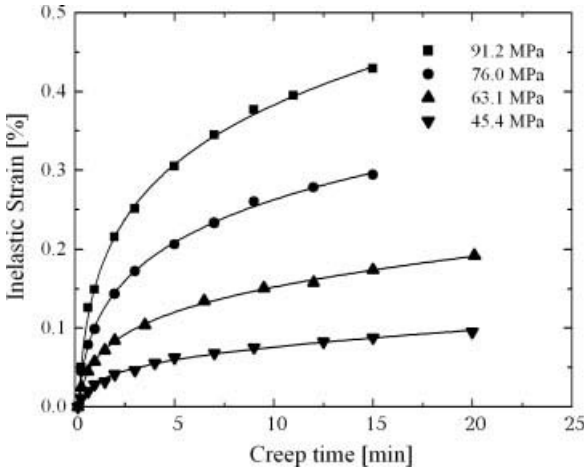

Figure 7. Experimental results of creep tests on PC at room temperature.

part with a constant deformation rate. For low stress levels, the rate of the secondary creep exhibits roughly exponential dependence on the applied stress, and a much stronger dependence can be observed when the applied load approaches the yield stress.

Our MC simulation reproduces similar creep behavior with a transient primary part and a linear secondary part (see Fig. 8). However, the dependence of the secondary creep rate on the applied stress is much weaker. The probable reason is the limited size of our model, which limits long-range interactions between PSTs. As a remedy to this problem, we varied the cutoff

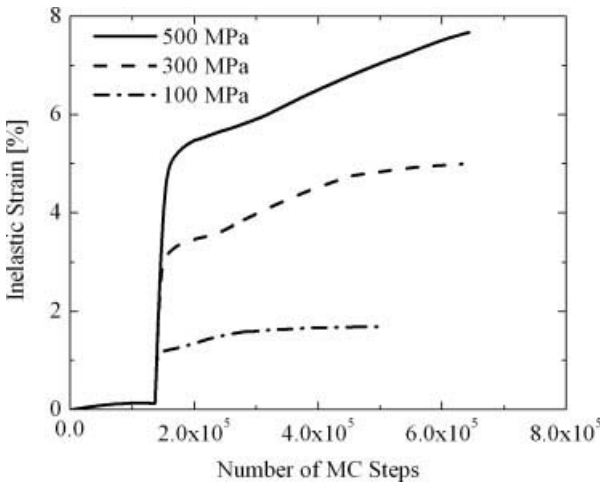

Figure 8. Results of the continuum-scale simulations. The transition from primary creep to secondary creep is sharper than that found in the experimental results.

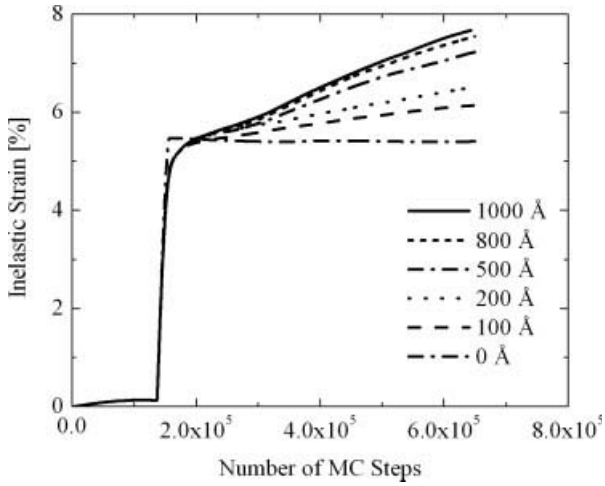

Figure 9. Results of the continuum-scale simulations. The slope of the secondary creep depends on the cutoff radius of the PST interactions.

radius for the interactions between the PSTs. Our results indicate that the secondary creep rate strongly depends on the cutoff radius (see Fig. 9). When the interactions between the PSTs were turned off (cutoff radius was set to zero), a zero secondary creep rate was observed. As the cutoff radius was increased, an increase was observed in the secondary creep rate. This indicates that during the initial stages of deformation in glasses, the interactions between localized defects can be responsible for plastic flow with a constant rate at a constant external stress.

CONCLUSIONS

We have studied the deformation of glassy polymers on two different length scales: atomistic and continuum. The simulations on the atomistic level were performed on PC with classical MD (with our own code Macromolecular Reality). The continuum-scale simulations were performed on a model glassy polymer with MC methodology and with the concept of PSTs. We have drawn the following conclusions:

- The local shear strains were calculated for each atom within a volume defined by their neighbors (with Voronoi tessellation). According to our definition (eq 1), the local shear strains can exceed the global shear strains substantially even when the global strains are elastic (<5%).

- Under uniaxial tension and compression, the local shear strain was highly localized. If the externally applied stress had a shear component, then the locally deformed regions merged to form flat elliptical regions with a high shear strain. These secondary structures were called PSTs.
- No such localization was observed under hydrostatic external loads.
- The nucleation of PSTs requires high atomic/segmental mobility and low (local) density.
- The plastic behavior of glasses can be simulated on the continuum scale, with PSTs being considered the basic region of deformation. The classic theory of elasticity can be used to calculate the internal energy of PSTs and interaction energy of PSTs with an external stress field as well as the energy of interaction between PSTs.
- Both primary creep behavior and secondary creep behavior were successfully reproduced with the proposed continuum-level approach.
- The slope of the secondary creep region depends on the cutoff radius of the interaction between PSTs.

The authors kindly acknowledge the financial support provided by the Office of Naval Research (grant N00014-01-10732), the National Science Foundation (CMS 0310596), and Rensselaer Polytechnic Institute to perform this work.

REFERENCES AND NOTES

1. Nabarro, F. R. N. Theory of Crystal Dislocations; Oxford University: Oxford, 1967.
2. Zeller, R. C.; Pohl, P. O. Phys Rev B 1971, 4, 2029.
3. Anderson, P. W.; Halperin, B. I.; Varma, C. M. Philos Mag 1972, 25, 1.
4. Phillips, W. A. J Low Temp Phys 1973, 11, 757.
5. Peierls, R. E. Proc Phys Soc London Sect A 1940, 52, 436.
6. Taylor, G. I. Proc R Soc London Ser A 1934, 145, 362.
7. Shenogin, S. V.; Hoehne, G. W. H.; Oleinik, E. F. Thermochim Acta 2002, 391, 13.
8. Oleinik, E. F.; Salamatina, O. B.; Rudnev, S. N.; Shenogin, S. V. Polym Sci A 1993, 35, 1819.
9. Gilman, J. J. J Appl Phys 1973, 44, 675.
10. Li, J. C. M.; Gilman, J. J. J Appl Phys 1970, 41, 4248.
11. Bowden, P. B.; Raha, S. Philos Mag 1974, 29, 149.
12. Argon, A. S. In Glass Science and Technology; Uhlman, D. R.; Kreidel, N. J., Eds.; Academic: New York, 1980; Vol. 5, p 79.
13. Spaepen, F. Acta Metall 1977, 25, 407.
14. Brady, T. E.; Yeh, G. S. Y. J Appl Phys 1971, 42, 4622.
15. Falk, M. L.; Langer, J. S. Phys Rev E 1998, 57, 7192.
16. Langer, J. S.; Pechenik, L. Phys Rev E 2003, 68, 061507.
17. Oleinik, E.; Shenogin, S.; Paramzina, T.; Rudnev, S.; Shantarovich, V.; Azamatova, Z.; Pakula, T.; Fischer, E. Polym Sci A 1998, 40, 1187.
18. Shantarovich, V. P.; Novikov, Y. A.; Suptel, Z. K.; Oleinik, E. F.; Boyce, M. C. Acta Phys Pol A 1999, 95, 659.
19. Wolff, J.; Franz, M.; Broska, A.; Kerl, R.; Weinhagen, M.; Kohler, B.; Brauer, M.; Faupel, F.; Hehenkamp, T. Intermetallics 1999, 7, 289.
20. Flores, K. M.; Suh, D.; Dauskardt, R. H.; Asoka-Kumar, P.; Sterne, P. A.; Howell, R. H. J Mater Res 2002, 17, 1153.
21. Utz, M.; Atallah, A. S.; Robyr, P.; Widmann, A. H.; Ernst, R. R.; Suter, U. W. Macromolecules 1999, 32, 6191.
22. Utz, M.; Robyr, P.; Suter, U. W. Macromolecules 2000, 33, 6808.
23. Loo, L. S.; Cohen, R. E.; Gleason, K. K. Macromolecules 1999, 32, 4359.
24. Mott, P. H.; Argon, A. S.; Suter, U. W. Polym Prepr 1989, 30, 34.
25. Argon, A. S.; Bulatov, V. V.; Mott, P. H.; Suter, U. W. J Rheol 1995, 39, 377.
26. Koteljanskii, M. Trends Polym Sci 1997, 5, 192.
27. van Workum, K.; de Pablo, J. J. Nano Lett 2003, 3, 1405.
28. Hutnik, M.; Argon, A. S.; Suter, U. W. Macromolecules 1993, 26, 1097.
29. Capaldi, F. M.; Boyce, M. C.; Rutledge, G. C. Polymer 2004, 45, 1391.
30. Yip, S.; Sylvester, M. F.; Argon, A. S. Comp Theor Polym Sci 2000, 10, 235.
31. Vellinga, W. P.; DeHosson, J. T. H. M.; Vitek, V. Acta Mater 1997, 45, 1525.
32. Abraham, F. F.; Broughton, J. Q.; Bernstein, N.; Kaxiras, E. Europhys Lett 1998, 44, 783.
33. Kohlhoff, S.; Gumbusch, P.; Fischmeister, H. F. Philos Mag A 1991, 64, 851.
34. Phillips, R. Curr Opin Solid State Mater Sci 1998, 3, 526.
35. Ortiz, M. Comput Mech 1996, 18, 321.
36. Tadmor, E. B.; Phillips, R.; Ortiz, M. Langmuir 1996, 12, 4529.
37. Tadmor, E. B.; Ortiz, M.; Phillips, R. Philos Mag A 1996, 73, 1529.
38. Shenoy, V. B.; Miller, R.; Tadmor, E. B.; Phillips, R.; Ortiz, M. Phys Rev Lett 1998, 80, 742.
39. Miller, R.; Phillips, R. Philos Mag A 1996, 73, 803.
40. Rafii-Tabar, H.; Hua, L.; Cross, M. J Phys: Condens Matter 1998, 10, 2375.

41. Gao, H.; Klein, P. J Mech Phys Solids 1998, 46, 187.
42. Hadjiconstantinou, N. G.; Patera, A. T. Int J Mod Phys C 1997, 8, 967.
43. Huber, G. A. Prog Biophys Mol Biol 1998, 69, 483.
44. Doruker, P.; Jernigan, R. L.; Bahar, I. J Comput Chem 2002, 23, 119.
45. See http://www.rpi.edu/~ozisik/ for more information.
46. Shenogin, S.; Ozisik, R. Presented at the American Physical Society Meeting, Austin, TX, March 2003; Paper C1.023.
47. Mapple, J. R.; Hwang, M. J.; Stockfish, T. P.; Dinur, U.; Waldman, M.; Ewing, C. S.; Hagler, A. T. J Comput Chem 1994, 15, 162.
48. (a) Sun, H. J Comput Chem 1994, 15, 752; (b) Sun, H. Macromolecules 1995, 28, 701; (c) Sun, H.; Mumby, S.; Hagler, A. T. J Am Chem Soc 1994, 116, 2978.
49. Muller, M.; Nievergelt, J.; Santos, S.; Suter, U. W. J Chem Phys 2001, 114, 9764.
50. Kremer, K.; Grest, G. S. J Chem Phys 1990, 92, 5057.
51. Yethiraj, A.; Hall, C. K. Macromolecules 1990, 23, 1865.
52. Brown, D.; Clarke, J. H. R.; Okuda, M.; Yamazaki, T. J Chem Phys 1994, 100, 6011.
53. Gao, J. J Chem Phys 1995, 102, 1074.
54. Mondello, M.; Grest, G. S.; Webb, E. B., III; Peczak, P. J Chem Phys 1998, 109, 798.
55. Kroger, M. Comput Phys Commun 1999, 118, 278.
56. Shenogin, S. V. Ph.D. Thesis, Russian Academy of Science, 1996.
57. Eshelby, J. D. In Progress in Solid Mechanics; Sneddon, I. N.;Hill, R., Eds.; North Holland: Amsterdam, 1961; Vol. 2, p 87.